International Journal on Magnetic Particle Imaging
Vol 3, No 2, Article ID 1706001, 7 Pages

Infinite Science Publishing

Research Article

Real-time 3D Dynamic Rotating Slice-Scanning Mode for Traveling Wave MPI

Patrick Vogel[a,b,*] · Martin A. Rückert[a] · Peter Klauer[a] · Stefan Herz[b] · Thomas Kampf[a,c] · Thorsten A. Bley[b] · Volker C. Behr[a]

[a] Department of Experimental Physics 5 (Biophysics), University of Würzburg, Würzburg, Germany
[b] Department of Diagnostic and Interventional Radiology, University Hospital Würzburg, Würzburg, Germany
[c] Department of Diagnostic and Interventional Neuroradiology, University Hospital Würzburg, Würzburg, Germany
[*] Corresponding author, email: patrick.vogel@physik.uni-wuerzburg.de

Received 25 November 2016; Accepted 20 March 2017; Published online 21 June 2017

Abstract

Magnetic Particle Imaging is a tomographic imaging technique offering high sensitivity and temporal resolution and is a promising tool for pre-clinical applications. The state of the art Traveling Wave Magnetic Particle Imaging (TWMPI) scanners offer a mouse-sized FOV, which can be scanned at once. Since the first introduction of TWMPI, several sequences have been introduced to scan the FOV in 2D as well as 3D. So far, the proposed 3D sequences do not provide real-time capability, which is an important feature for future clinical applications such as guided vascular interventions. In this study a modified sequence for TWMPI scanners is presented, which allows scanning an entire 3D volume on a short time scale. Furthermore, for real-time capability a novel reconstruction method using an image-based approach is used providing a 3D visualization in real-time.

I. Introduction

Magnetic Particle Imaging (MPI) was introduced in 2005 by B. Gleich and J. Weizenecker [1]. This novel technique is based on the nonlinear response of superparamagnetic iron-oxide nanoparticles (SPIONs) to dynamic magnetic fields. For imaging, a strong gradient field has to be applied offering a selective signal generation. This field-free point (FPP) is steered through the volume of interest and the spatial distribution of SPIONs can be reconstructed. In first experiments the 3D data acquisition ability with 46 volumes per second were demonstrated [2], followed by optimizing the reconstruction process for visualizing the acquired data in almost real-time [3]. However, state-of-the-art software implementations struggle with a delay time of about 2.3 s [3].

The Traveling Wave MPI (TWMPI) scanner is one of many scanner types, which have been developed during the last decade [4]. TWMPI uses an array of multiple electro coils (dynamic linear gradient array - dLGA) for generating and moving the required magnetic fields with the main frequency f_1 providing a large FOV sufficient to cover a mouse-sized sample [5]. Two perpendicular saddle coil systems are used for steering the FFPs arbitrarily through the FOV. Since the first publication of TWMPI several sequences have been introduced to steer the FFP along different trajectories through the FOV covering large volumes of interest [5–7]. The rotating slice-scanning mode (rSSM) [8] is the latest sequence for covering a 3D volume by rotating scanning-slices step-by-step around the z-axis (Fig. 1 a–c). In this approach both saddle coil systems are driven with the same frequency f_2 ($f_2 \gg f_1$) and same phase but with different amplitudes suitable to the angle β of the desired scanning-slice (Fig. 1 d, left). For a 3D reconstruction every slice is handled separately and combined in a final step. For reconstructing every single 2D image a Wiener filter and the system specific point spread function (PSF) are used (deconvolution reconstruction method) [8]. There is also an image-based reconstruction method available,

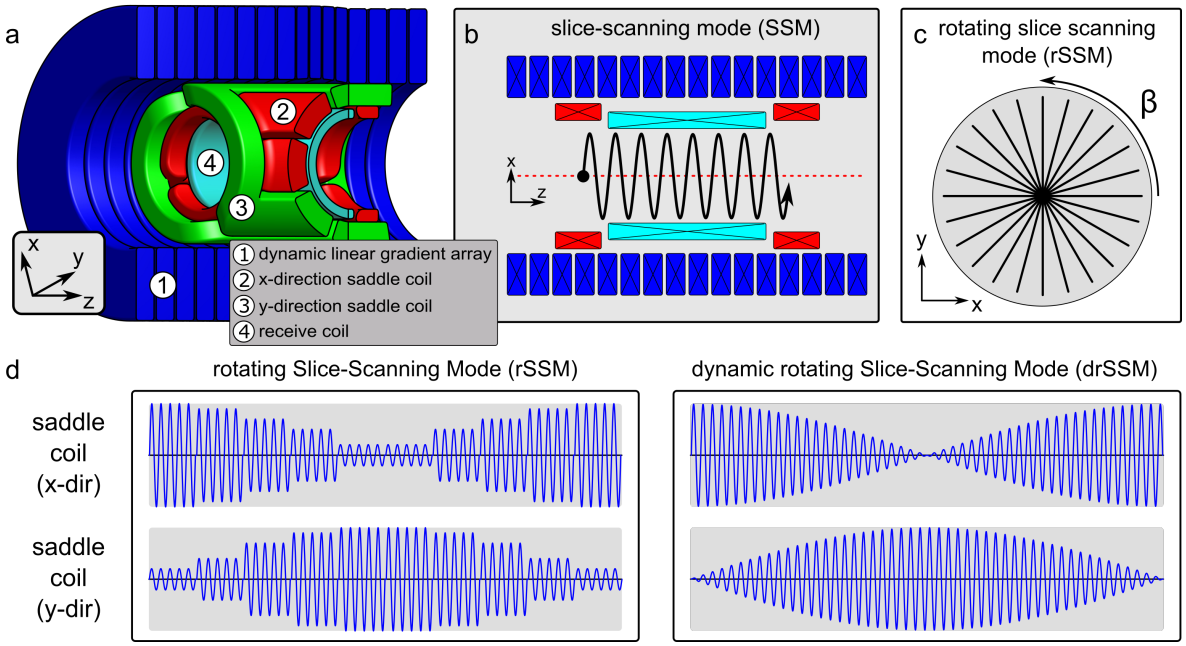

Figure 1: (a) sketch of the TWMPI scanner consisting of (1) the dynamic linear gradient array (dLGA), two perpendicular saddle coil systems (2),(3) and the receive coil (4). (b) shows the slice-scanning mode (SSM), where the FFPs are traveling along a sinusoidal trajectory on a plane through the FOV. For scanning a 3D volume the scanning-slice is rotated step-by-step around the z-axis (rotating slice-scanning mode - rSSM). (d) Sequence table for rSSM and dynamic rSSM.

which uses a system matrix approach [9] based on images, which allows reconstructing highly resolved areas in a fast way and with reduced computational effort [10]. However, every scanning-slice in rSSM is acquired in burst-mode [6–8], which means scanning the dedicated slice with multiple periods of f1. With the ratio of the frequencies f_1 and f_2 ensuring a slightly different trajectory for each period results in an increase of pixels. This can be used for gridding highly resolved (extrinsic resolution) raw-images providing a better signal-to-noise ratio (SNR) [7]. A more prominent obstacle is the discontinuous hardware switching between two scanning-slices, which can influence the performance of the receive chain. This problem can be solved by adding a dead time between two scanning-slice sequences.

Both workarounds increase the scanning time for an entire 3D volume dramatically, e.g. a 3D volume scanned with 72 slices each taking 20 ms and a required dead time of about 20 ms results in an acquisition time of about 2.88 s.

Since the TWMPI system is able to scan one slice in a very short time (up to 1840 frames per second in continuous scanning mode) [11], the theoretical scanning time t_{3D} for a 3D volume using the rSSM method grows linearly with the number of appointed scanning-slices n_{slice}:

$$t_{3D} = n_{slice} \cdot 1/f_1 \,. \tag{1}$$

One drawback of the continuous scanning mode is the resulting low SNR and reduced extrinsic resolution resulting from scanning in such a short time, e.g. TWMPI scanner driven in SSM at $f_1 = 1$ kHz, results in a scanning time of 0.5 ms per image and 50k data points for one slice ($SR = 100$ MS/s).

In this work, a modified trajectory is presented, which rotates the scanning-slices continuously covering an entire 3D volume within a single shot. This sampling path is comparable with the concepts of elongated trajectories shown by Kaethner et al. [12].

Furthermore, an image-based system matrix reconstruction approach is introduced providing three-dimensional real-time reconstruction capability.

II. Methods

II.I. Dynamic rSSM

This modified sequence is based on the rotating slice scanning mode (rSSM), but instead of rotating every scanning-slice step-by-step (Fig. 1 d, left), both saddle coil systems are driven continuously with the frequency f_2 ($f_2 \gg f_1$) and the amplitude of both coils is modulated with a frequency f_3 ($f_3 \ll f_1$) (see Fig. 1 d, right). In the following control matrix, the sequence is given for all

four channels of a TWMPI scanner (CH1 and CH2 for dLGA, CH3 for saddle coil in x-direction, and CH4 for saddle coil in y-direction):

$$\begin{aligned} \mathrm{CH1}: s_1 &= A_1 \cdot \sin\left(2\pi \cdot f_1\right) \\ \mathrm{CH2}: s_2 &= A_1 \cdot \cos\left(2\pi \cdot f_1\right) \\ \mathrm{CH3}: s_3 &= A_2 \cdot \sin\left(2\pi \cdot f_2\right) \cdot \sin\left(2\pi \cdot f_3\right) \\ \mathrm{CH4}: s_4 &= A_2 \cdot \sin\left(2\pi \cdot f_2\right) \cdot \cos\left(2\pi \cdot f_3\right) \end{aligned} \tag{2}$$

As a result, the FFP moves in a plane slowly twisted along z-axis (see Fig. 2). The frequency f_3 is adjusted in a way that for one complete 3D scan t_{3D} the scanning-slice rotates around 360 degree:

$$f_3 = \frac{1}{t_{3D}} = \frac{f_1}{n_{slice}}. \tag{3}$$

For example, scanning an entire 3D volume in $t_{3D} = 20\,\mathrm{ms}$ ($n_{slice} = 20$ and $f_1 = 1\,\mathrm{kHz}$) requires a modulation frequency of $f_3 = 50\,\mathrm{Hz}$. That means in 20 ms the FFPs travel 20 times through the FOV on slightly rotated slices. However, since the rotation of the slice is performed continuously, the slices should be renamed to twisted slices. For the reconstruction process only the continuity, not the rotation speed is important due to the gridding process.

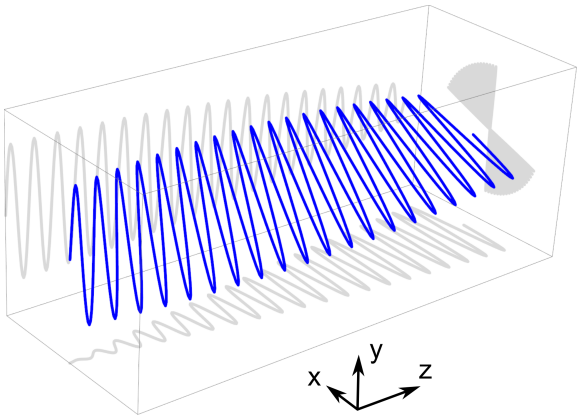

Figure 2: Trajectory (blue) of the FFP twisted around the z-axis. The projections (gray) support the view and give the amplitude for CH3 and CH4 (see Fig. 1 d, right).

II.II. Reconstruction process

The reconstruction process for this method is quite similar to the method used for SSM [6, 7] or rSSM [8]. In a first step the input data were corrected for the receive chain distortion (receive chain correction - RCC) and filtered (band pass) afterwards before they were gridded on a 2D image to generate the raw-images, which can be reconstructed using deconvolution [6–8] or system matrix approach [10].

For the proposed method, the entire data of all twisted slices were concatenated into a single raw-image instead processing each slice separately.

II.II.1. 2D gridding of 3D data

For the reconstruction an image-based approach was used [6–8]. The time domain data were continuously gridded point-by-point on a surface [13, 14], where the x-direction corresponds to the phase of f_2 and the y-direction to f_3 or t_{3D} (compared to SSM: x-dir: f_2 and y-dir: f_1) (see Fig. 3 b). Since in x-direction the data were gridded for a full period, the information of the left and right side is identical (back- and forth-scan). Thus, both sites can be combined to increase the extrinsic resolution of the raw-image. This results in a raw-image which consists of the stacked twisted raw-slices (twisted slices) of the single FFP passages through the FOV (Fig. 3 c: cyan and green areas). Each area represents the signal collected by a FFP traveling the entire length of the FOV (half period of f_1). Due to the slow rotation of the scanning-slice, each region can be seen approximately as single scanning-slices of the FOV with slightly different angles (see Fig. 1 c and Fig. 2).

The size (or extrinsic resolution) of the raw-images can be chosen arbitrarily with possible empty space between gridded data points representing the trajectory being filled up by a linear interpolation algorithm [10].

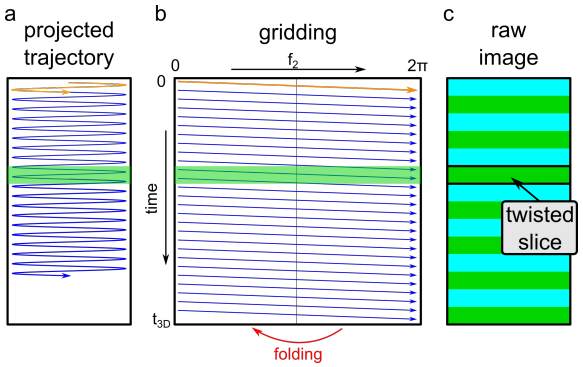

Figure 3: (a) For the gridding process the twisted trajectory over the entire time can be mapped on a 2D surface. (b) The input data set is gridded point-by-point on the 2D surface, where the axes correspond to the frequencies f_2 and f_3 or t_{3D} respectively. By folding, the extrinsic resolution of the raw-image can be increased. (c) After gridding, the raw-image consists of concatenated scanning-slices (twisted slices) (see Fig. 2).

Finally, the resulting raw-image shows the untwisted or mapped 3D data on a 2D surface. From this state, the reconstruction process can be performed using the image-based system matrix reconstruction approach proposed in [10].

10.18416/ijmpi.2017.1706001

II.II.2. Image-based reconstruction using a dedicated system matrix

For reconstruction using the system matrix approach, a measurement-based [9] or a model-based [15] system matrix can be used. For the first one a delta-like probe is placed on each spatial position in the FOV and measured, while for the second one the signal for each position is calculated in an simulation environment [16] emulating the MPI system.

For building the system matrix from n data sets several methods are available [10]. Finally, the reconstruction of the image can be performed by solving the inversion of the system matrix [9].

According to the image-based system matrix reconstruction method shown in [10], for each position the raw-image is generated as proposed in Sec. II.II.1 before the values of each raw-image were written pixel-by-pixel into a system matrix with the size $m \times n$ (see Fig. 4).

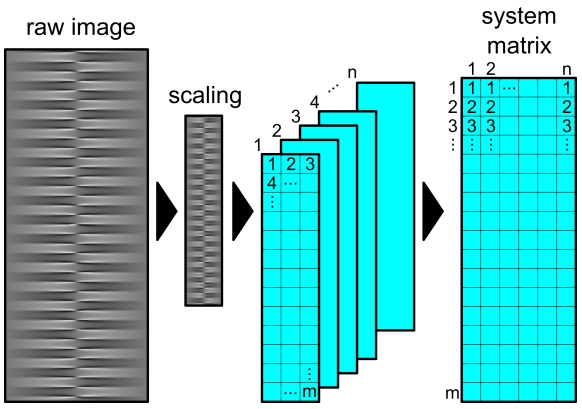

Figure 4: Image-based reconstruction method: in a first step, the raw-image is scaled down to an appropriate size, before every pixel of the n data sets is written to a system matrix with the size $m \times n$.

For the final reconstruction step, the inversion of the system matrix has to be calculated and multiplied with the prepared measured or simulated data set [17–19].

II.II.3. 3D mapping

According to the order of their positions, the delta-like signals were measured or generated, an appropriate look-up-table can be built to transform the reconstructed 2D data in a 3D volume (see Fig. 5).

II.III. Simulation

For an initial test, an entire 3D system matrix was simulated for a TWMPI system using a custom simulation software [16]. The parameters for the simulated TWMPI scanner were taken from the real scanner [7]: FOV size of $65 \times 25 \times 25\,\mathrm{mm}^3$, gradient strength of 4 T/m (z-direction) and working frequencies $f_1 = 920\,\mathrm{Hz}$, $f_2 = 16823\,\mathrm{Hz}$, and

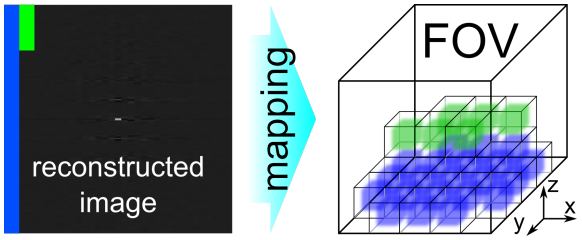

Figure 5: Using a system matrix reconstruction method the reconstructed image is created containing the 3D data, which can be mapped in a 3D space using an appropriate coordinate look-up-table.

$f_3 = 50\,\mathrm{Hz}$. The FOV is discretized in $15 \times 15 \times 35$ voxels (cylinder shaped) corresponding to an isotropic voxel size of about 2 mm. This results in 35 almost circular slices arranged along the z-direction with 177 voxels per slice resulting in 6195 voxels for the entire 3D volume (see Fig. 6 d). The order of the positions of the delta-like samples goes along the x-, y-, and z-direction, which results in a look-up table, where the column (y-direction) of the reconstructed image represents one cylindrical slice (see Fig. 6 b).

Since the extrinsic resolution of the raw-image should be chosen in a way that the data points are preferably equally distributed using the drSSM gridding process, the raw-images here provide more pixels in height as in width ($600 \times 740\,\mathrm{px}^2$ and after combining redundant data $300 \times 740\,\mathrm{px}^2$).

For the following steps of the reconstruction process, the size of the raw-image has to be decreased to be manageable, e.g. system matrices with a size of $(300 \times 370 = 111000) \times 6195$ entries are hardly computable and also overdetermined [10].

Thus, the raw-images were scaled-down to a size of $58 \times 177\,\mathrm{px}^2$ [10]. This results in a system matrix with 15370×6195 entries.

III. Results

The results of a simulation of a line sample can be seen in Fig. 6 starting with the raw-image (Fig. 6 a). A closer look makes the line-shaped sample visible for each region corresponding to the signal the FFPs collected in a full period (see Fig. 2 and Fig. 3 c). The reconstruction process using the simulated system matrix (truncation level[1]: 2500) creates a final reconstructed 2D image (Fig. 6 b) representing the values for the voxels in the same order the system matrix was simulated (here: horizontal means z-direction with 35 entries and vertical means x-/y-direction with 177 entries). A suitable coordinate

[1] Truncation level denotes the number of used singular values for matrix inversion: by using singular value decomposition [18] for calculating the pseudo inverse of the system matrix, it is possible to 'filter' inappropriate data by truncation or weighting [17].

look-up table (Fig. 6 d) is used to fill up a 3D volume to visualize the FOV in three dimensions (Fig. 6 c) using a custom 3D visualization tool.

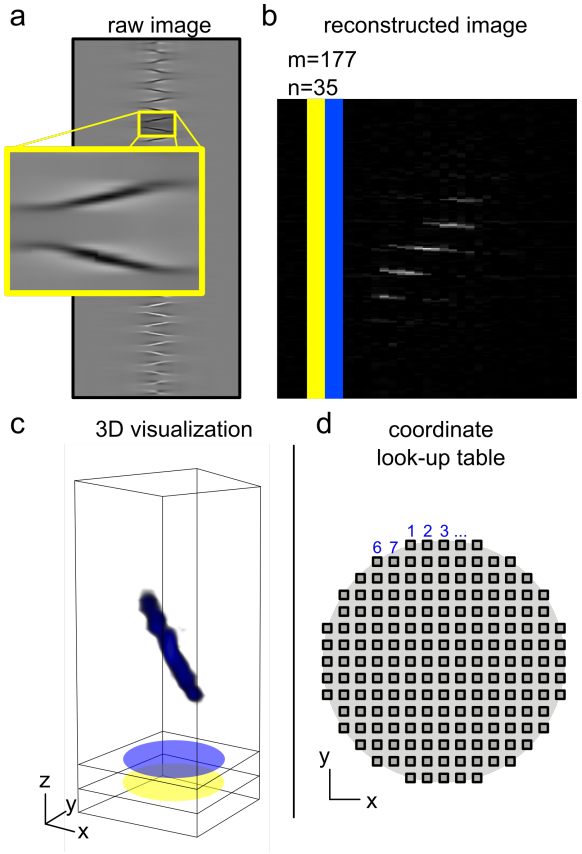

Figure 6: Reconstruction steps for a simulated line sample: (a) shows the raw-image, where the line-shape is visible for every region representing a scanning-slice. (b) After reconstruction using the corresponding system matrix the final image is created. (c)(d) By re-ordering the 2D data using a suitable coordinate look-up table the data values can be mapped into a 3D volume to visualize the 3D FOV.

III.I. Encoding capability

To get an idea of the encoding capability of this novel scanning method, it is important to have a closer look at the system function (sf) given by the simulated system matrix. For that every data set of each spatial position is Fourier transformed and signal distribution can be visualized for every frequency (real, imaginary or absolute values).

Since drSSM works with three excitation frequencies, the spectrum of each data set shows a bunch of specific higher harmonics and their mixed components. In Fig. 7 a selection is given showing the system functions for several frequencies. In a first view, there are basically two different structures available: a pancake-like structure (Fig. 7 left) and a spiral structure (Fig. 7 right).

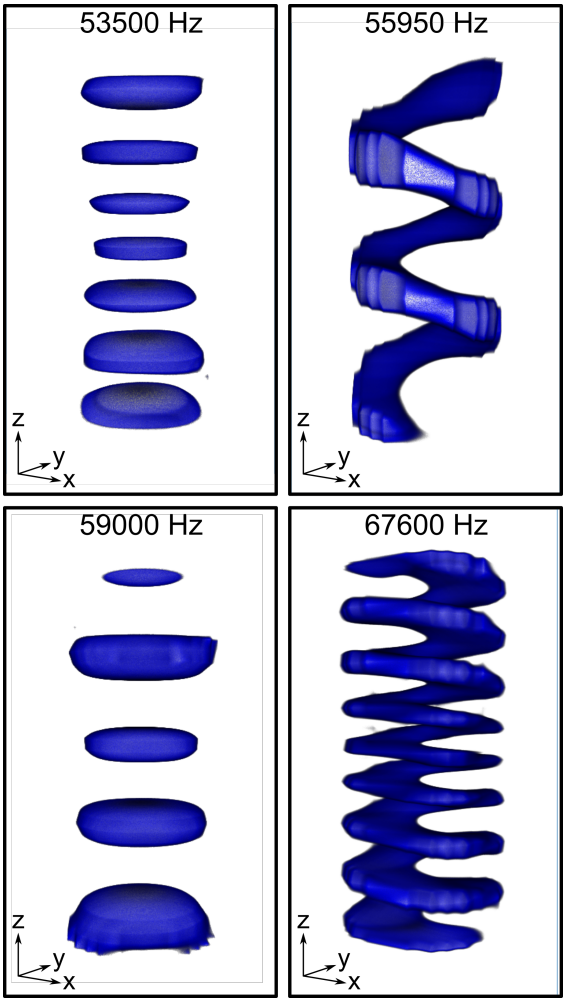

Figure 7: Visualization of several system functions at the frequencies 53500 Hz, 55950 Hz, 59000 Hz, and 67600 Hz. The simulation for the system matrix was performed with the following settings: $f_1 = 920$ Hz, $f_2 = 16823$ Hz, and $f_3 = 50$ Hz.

III.II. Real-time capability

The entire reconstruction process contains several calculation steps:

Correction step: after data transfer from the analog-digital-converter (ADC), the data sets are corrected (receive-chain distortions) and filtered.

Gridding step: the corrected data is gridded using a pre-calculated scheme depending on the excitation frequencies to provide the raw-image.

Reconstruction step: for the reconstruction using an image-based system matrix, the raw image is prepared (scaled down) and multiplied with the pre-calculated pseudo inverse of the system matrix.

Running the sequence, transferring data, and finally mapping the 2D reconstructed data in a 3D volume for visualization prolongates image acquisition time. In Tab. 1 an overview is given that shows the time values for every step.

10.18416/ijmpi.2017.1706001

The total computation time including sequence and data transfer is about 180 ms (see Tab. 1 for hardware configuration) and the pure reconstruction time is in the range of about 115 ms (without sequence, data transfer from the ADC, and 2D visualization).

Table 1: Overview about time values for every step. Correction time (Fast Fourier Transform (FFT), correction, inverse FFT), gridding and reconstruction (data preparation and matrix multiplication) steps were determined on an i7 4750HQ. [1)] The time values depend on the length of the sequence. [2)] Transfer time for a data set with $2 \cdot 10^6$ data points from HDO8038 (Teledyne LeCroy, USA) to reconstruction software.

Step	Time [ms]
Sequence	20+[1)]
Data transfer	∼35[2)]
Correction	∼30
Gridding	∼25
Reconstruction	∼60
3D Visualization	∼10
$\sum$	**180+**

IV. Discussion

The system matrix used in this study has a size of 15370 × 6195 representing 6195 voxels in a 3D FOV. This corresponds to an isotropic voxel size of about 2 mm. Improving the resolution of the system matrix further to e.g. 1 mm will increase the number of voxels to approximately 50000 resulting in a huge system matrix, which is difficult to handle [10].

In Tab. 1 it can be seen, that the major time loss is the reconstruction process, which is primarily caused by matrix multiplication. Decreasing the size of the system matrix increases the reconstruction time but also decreases the amount of voxels in the FOV.

However, the flexible patch reconstruction method introduced in [5] uses only small areas and allows the reconstruction of parts of images separately resulting in a less calculation effort.

This technique can also be applied on a drSSM raw-image. The selection of an area in a single scanning-slice (twisted slice) results in a simultaneous selection of this area on all other slices resulting in a 3D cylindrical patch, which can be reconstructed with a higher resolution in a shorter time (see Fig. 8).

A further improvement of the reconstruction speed is the possibility of parallelizing. For that, every twisted slice can be processed separately and multiplied with an appropriate smaller pseudo inverse. E.g. a raw-image of the size $100 \times 1000\,\mathrm{px}^2$ containing 20 twisted slices representing 40000 voxels results in a calculation of 20 times a system matrix with the size of 5000 × 2000 instead of calculating one system matrix with the size of 100000 × 40000.

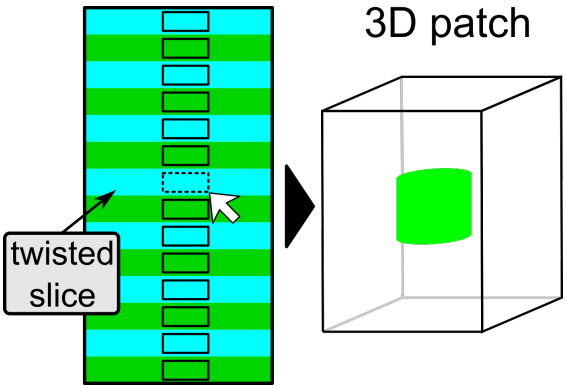

Figure 8: Flexible patch reconstruction method applied on a drSSM raw image. By choosing the area of interest, the same areas are selected simultaneously on all other slices resulting in a 3D patch.

V. Conclusion

In this study, a modified sequence for TWMPI scanners is presented, which allows scanning an entire 3D volume with short acquisition time. The presented dynamic rotating slice-scanning mode (drSSM) is quite similar to the rotating slice-scanning mode (rSSM) but rotates the scanning-slice continuously around the z-axis. This approach results in a fast coverage of the FOV and offers the possibility of using a fast image-based reconstruction method to visualize them in 3D in real-time with approximately 5 volumes per second.

This approach decouples the hardware (signal acquisition) from the reconstruction process [10]. Therefore several parameters like sampling rate or trigger point can be set arbitrarily, which simplifies working with same reconstruction settings on data generated within the same type of scanner but with different parameters (frequencies, or sampling rate).

This approach offers the possibility for near real-time imaging of 3D volumes. This could be an interesting tool for future clinical applications such as guided vascular interventions.

Acknowledgements

This work was partially funded by the DFG (BE-5293/1-1).

References

[1] B. Gleich and J. Weizenecker. Tomographic imaging using the nonlinear response of magnetic particles. *Nature*, 435(7046):1214–1217, 2005. doi:10.1038/nature03808.

[2] J. Weizenecker, B. Gleich, J. Rahmer, H. Dahnke, and J. Borgert. Three-dimensional real-time in vivo magnetic particle imaging. *Phys. Med. Biol.*, 54(5):L1–L10, 2009.

[3] T. Knopp and M. Hofmann. Online reconstruction of 3D magnetic particle imaging data. *Phys. Med. Biol.*, 61(11):N257–N267, 2016. doi:10.1088/0031-9155/61/11/N257.

[4] N. Panagiotopoulos, R. L. Duschka, M. Ahlborg, G. Bringout, C. Debbeler, M. Graeser, C. Kaethner, K. Lüdtke-Buzug, H. Medimagh, J. Stelzner, T. M. Buzug, J. Barkhausen, F. M. Vogt, and J. Haegele. Magnetic particle imaging: current developments and future directions. *Int. Journ. Nanomed.*, 10:3097, 2015. doi:10.2147/IJN.S70488.

[5] P. Vogel, M. A. Rückert, P. Klauer, W. H. Kullmann, P. M. Jakob, and V. C. Behr. Traveling Wave Magnetic Particle Imaging. *IEEE Trans. Med. Imag.*, 33(2):400–407, 2014. doi:10.1109/TMI.2013.2285472.

[6] P. Vogel, S. Lother, M.A. Ruckert, W.H. Kullmann, P.M. Jakob, F. Fidler, and V.C. Behr. MRI Meets MPI: A Bimodal MPI-MRI Tomograph. *IEEE Trans. Med. Imag.*, 33(10):1954–1959, 2014. doi:10.1109/TMI.2014.2327515.

[7] P. Vogel, M. A. Rückert, P. Klauer, W. H. Kullmann, P. M. Jakob, and V. C. Behr. First in vivo traveling wave magnetic particle imaging of a beating mouse heart. *Phys. Med. Biol.*, 61(18):6620–6634, 2016. doi:10.1088/0031-9155/61/18/6620.

[8] P. Vogel, M. A. Rückert, P. Klauer, W. H. Kullmann, P. M. Jakob, and V. C. Behr. Rotating Slice Scanning Mode for Traveling Wave Magnetic Particle Imaging. *IEEE Trans. Magn.*, 51(2):6501503, 2015. doi:10.1109/TMAG.2014.2335255.

[9] J. Rahmer, J. Weizenecker, B. Gleich, and J. Borgert. Signal encoding in magnetic particle imaging: properties of the system function. *BMC Medical Imaging*, 9(4), 2009. doi:10.1186/1471-2342-9-4.

[10] P. Vogel, T. Kampf, M. A. Rückert, and V. C. Behr. Flexible and Dynamic Patch Reconstruction for Traveling Wave Magnetic Particle Imaging. *Intern. J. Magnetic Particle Imaging*, 2(2):1611001, 2016. doi:10.18416/ijmpi.2016.1611001.

[11] P. Vogel, M. A. Rückert, P. Klauer, W. H. Kullmann, P. M. Jakob, and V. C. Behr. Superspeed Traveling Wave Magnetic Particle Imaging. *IEEE Trans. Magn.*, 51(2):6501603, 2015. doi:10.1109/TMAG.2014.2322897.

[12] C. Kaethner, M. Ahlborg, G. Bringout, M. Weber, and T. M. Buzug. Axially Elongated Field-Free Point Data Acquisition in Magnetic Particle Imaging. *IEEE Trans. Med. Imag.*, 34(2):381–387, 2015. doi:10.1109/TMI.2014.2357077.

[13] P. W. Goodwill and S. M. Conolly. The x-Space Formulation of the Magnetic Particle Imaging process: One-Dimensional Signal, Resolution, Bandwidth, SNR, SAR, and Magnetostimulation. *IEEE Trans. Med. Imag.*, 29(11):1851–1859, 2010. doi:10.1109/TMI.2010.2052284.

[14] P. W. Goodwill and S. M. Conolly. Multidimensional X-Space Magnetic Particle Imaging. *IEEE Trans. Med. Imag.*, 30(9):1581–1590, 2011. doi:10.1109/TMI.2011.2125982.

[15] T. Knopp, T. F. Sattel, S. Biederer, J. Rahmer, J. Weizenecker, B. Gleich, J. Borgert, and T. M. Buzug. Model-Based Reconstruction for Magnetic Particle Imaging. *IEEE Trans. Med. Imag.*, 29(1):12–18, 2009. doi:10.1109/TMI.2009.2021612.

[16] P. Vogel, M. A. Rückert, and V. C. Behr. 3D-GUI Simulation Environment for MPI. In *International Workshop on Magnetic Particle Imaging*, 2016.

[17] T. Knopp, J. Rahmer, T. F. Sattel, S. Biederer, J. Weizenecker, B. Gleich, J. Borgert, and T. M. Buzug. Weighted iterative reconstruction for magnetic particle imaging. *Phys. Med. Biol.*, 55(6):1577–1589, 2010. doi:10.1088/0031-9155/55/6/003.

[18] D. Kalman. A Singularly Valuable Decomposition: The SVD of a Matrix. *College Math. J.*, 27(1):2–23, 1996. doi:10.2307/2687269.

[19] P. C. Hansen. *Rank-Deficient and Discrete Ill-Posed Problems: Numerical Aspects of Linear Inversion.* SIAM, Philadelphia, 1998. doi:10.1137/1.9780898719697.

